Coumarin-based Fluorescent Probes for Selectively Targeting and Imaging the Endoplasmic Reticulum in Mammalian Cells

Chamari S. Wijesooriya[1], Megan Nieszala[2], Alex Stafford[2], Jake R. Zimmerman[2], Emily A. Smith*[1]

[1] Department of Chemistry, Iowa State University, Ames, IA 50011, USA, [2] Department of Chemistry and Biochemistry, Ohio Northern University, Ada, OH 45810, USA

*Corresponding author e-mail: esmith1@iastate.edu (Emily A. Smith)

ABSTRACT

Developing improved fluorescent probes for imaging the endoplasmic reticulum (ER) is necessary for structure-activity studies of this dynamic organelle. Two coumarin-based compounds with sulfonamide side groups were synthesized and characterized as ER-targeting probes. Their selectivity to target the ER in HeLa and GM07373 mammalian cells was shown with co-localization experiments using commercially available probes that localize in the ER, mitochondria, or lysozymes. The hydrophobicity of the coumarin-based probes was comparable to known probes that partition into the ER membrane. Their cytotoxity in mammalian cells was low with IC50 values that range from 205-252 μM. The fluorescent quantum yields of the coumarin-based probes when excited with 400 nm light were 0.60, and they have a much narrower emission spectrum (from 435-525 nm in methanol) than that of the only commercially available ER probe that is exited with 400 nm light (ER-Tracker™ Blue-White DPX). Thus, the coumarin-based probes are more useful for multicolor imaging with yellow and red emitting fluorophores. In addition to the above benefits, ER labeling was achieved with the coumarin-based probes in both live cells and fixed cells, revealing their versatility for a wide range of cellular imaging applications.

INTRODUCTION

The endoplasmic reticulum (ER) is the largest organelle in most eukaryotic cells (*1, 2*). It consists of a network of tubules and sacs enclosed with a continuous single lipid membrane that constitutes approximately half of the total area of lipid membranes in the cell (*3*). The ER plays a vital role in maintaining cellular processes, including posttranslational processing, folding and trafficking of proteins into other organelles (*4*) and synthesizing lipids (*5*). It is also responsible for stabilizing the intracellular calcium concentration (*6*). There are two structurally and functionally distinct components of the ER. Processes related to protein modification occur in the rough ER, which is a stacked sheet-like structure located in the perinuclear region of the cell. The smooth ER consists of a tubular component extending from the rough ER throughout the cytoplasm and is involved in lipid metabolism (*1*).

Several physiological conditions such as oxygen deficiency, altered glucose and calcium levels, excessive acidity as well as some pathological conditions can alter protein folding in the ER (*7*). This results in the accumulation of unfolded or misfolded proteins in the ER lumen and generates stress, which alters the size of the ER structure. Specially, the sheet-like structures expand (*8*). Visualizing this dynamic organelle is important to understand the relationship between its structure and biological activity (*9*).

Fluorescence imaging is a non-invasive and versatile technique for imaging cellular organelles, including the ER. The commercially available ER targeting probes (ER-Tracker™ Blue-White DPX, ER-Tracker™ Green/BODIPY™ FL Glibenclamide, and ER-Tracker™ Red/BODIPY™ TR Glibenclamide) shown in Figure **S1** contain the sulfonamide group in their structures, and are targeted to the sulfonylurea receptors on the ER membrane (*10*).

Several recently reported ER-targeting probes contain a sulfonamide linker attached to a fluorophore (*11-13*). Due to the lower cholesterol composition in the ER membrane (*14*), moderately lipophilic fluorescent probes such as ER Thermo Yellow (*15*) and BODIPY Nile Red (*16*) have been identified to selectively accumulate in the ER. Carbocyanine fluorophores such as DiOC6 and DiOC5 also have also been reported to target the ER membrane (*17*), but they are not selective for ER imaging because they are also retained in other cellular organelles (*18*). Developing ER probes emitting at different wavelengths is important for multicolor imaging (e.g., dual labeling). Among the currently available commercial ER probes, ER-Tracker™ Blue-White DPX is excited around 400 nm (*19, 20*). This probe, however, has a very broad emission profile ranging from 430-640 nm, and is not very useful for multicolor imaging with other fluorescent probes. Another disadvantage of commercial ER probes is their high cost due in part to their complex synthesis procedures.

<Figure 1>

Herein we introduce two coumarin-based compounds as ER-selective fluorescent probes (Figure **1**, Compound **1a** and **1b**). Previous studies showed that the methoxy group attached to the sulfonamido side group had a higher membrane permeability than the methyl group attached at the same position (*21*). Therefore, we studied compounds 1a and 1b with methyl and methoxy groups attached to the sulfonamide side group, respectively. The synthesis of the probes involves a simple two-step process based on an inverse-demand hetero-Diels-Alder reaction. The probe has low toxicity in HeLa and GM07373 mammalian cell lines. Its excitation is around 400 nm and it has a narrower emission range (from 435-525 nm in methanol) compared to ER-Tracker™ Blue-White DPX. These coumarin-based probes will be

valuable imaging tools for tracking the ER structure over time due to their selectivity, low cytotoxicity, bright emission in the blue region and the simple synthetic procedure.

MATERIALS AND METHODS

Synthesis: 7-Diethylamino-3-formylcoumarin, methyl trimethylsilyl dimethylketene acetal, sulfonamides and solvents were purchased from Sigma-Aldrich and Acros and used without further purification. 7-Diethylamino-3-formylcoumarin (**1**) (0.5 mmol), sulfonamide (0.6 mmol) (p-methyl or p-methoxy sulfonamide), pyridinium p-tolunesulfonate (PPTS) (0.1 mmol), molecular sieves (MS4Å), and toluene (5 mL) were added to a 25 mL round bottom flask. The flask was then equipped with a condenser, and the reaction was heated to reflux in an oil bath. After approximately 18-24 h the reaction was cooled to room temperature and then to 0 ˚C. The resulting bright red solid was filtered off and was then immediately transferred to a new 25 mL round bottom flask. Dichloromethane (2 mL) and THF (2 mL) were then added followed by methyl trimethylsilyl dimethylketene acetal (2.5 mmol) and $Y(OTf)_3$ (0.1 mmol). The reaction was stirred at room temperature for 20-30 min until it was deemed complete via monitoring by TLC. The reaction was quenched on a pad of silica (~1g), the solvent was evaporated and the crude mixture was purified via column chromatography (30% EtOAc/70% hexanes ramped to 100% ethyl acetate).

^{1}H-NMR were recorded on a Bruker Advance 400 MHz instrument (Figure **S2**). Chemical shifts are reported in parts per million (ppm) down field from TMS, using residual $CDCl_3$ (7.27 ppm) as an internal standard. Data are reported as follows: Chemical shift, multiplicity (s

= singlet, d = doublet, t = triplet, q = quartet, m = multiplet, dd = doublet of doublet, bs = broad singlet), coupling constant and integration. ^{13}C-NMR was recorded on a Bruker Advance 400 MHz (100 MHz) instrument using broadband proton decoupling (Figure **S3**). Chemical shifts are reported in parts per million (ppm) downfield from TMS, using the middle resonance of $CDCl_3$ (77.0) as an internal standard. Infrared spectra were recorded on a Thermofisher IR100 FTIR instrument using NaCl pellets. Absorption peaks are given in wavenumbers (cm^{-1}). Flash chromatography was performed using a CombiFlash® Companion (Teledyne-Isco) chromatography system with RediSep® (Teledyne-Isco) disposable flash chromatography columns. High resolution mass spectra were collected using the Agilent QTOF 6540 (Santa Clara, CA) mass spectrometer, equipped with an Agilent LC 1200 series HPLC system (Figure **S4**).

Characterization of the optical properties of Compound 1a and 1b: Absorbance and fluorescence spectra of Compound **1a** and **1b** (3 μM) in different solvents were obtained using the Agilent 8453 UV-vis spectrophotometer (Santa Clara, CA) and FluoroMax-4 spectrofluorometer (Jobin Yvon Horiba), respectively. Emission spectra of Compound **1a** and **1b** in HeLa cells were measured using a Nikon Eclipse Ti microscope (Melville, NY) operated in a wide-field, epi-fluorescence mode with a Kymera 193i adaptive focus imaging spectrograph and Newton CCD camera (Andor, Belfast, UK).

Coumarin 153 was used as the standard (Φ_{fl}=0.53, ethanol) to measure the fluorescence quantum yields of Compound **1a** and **1b**. A series of concentrations of Compounds **1a** and **1b** (0.05 μM- 0.5 μM) and coumarin 153 (0.05 μM- 0.5 μM) were prepared in ethanol and the absorbance spectra and the fluorescence spectra at 400 nm excitation were determined. Calibration curves were prepared by plotting the integrated fluorescence intensity vs

absorbance at 400 nm, and were fit using a linear least squares regression. The slope of the fit line was used to calculate the fluorescence quantum yield using the following equation.

$$\Phi_{\mathbf{x}} = \Phi_{\mathbf{std}} \left(\frac{\mathbf{slope_x}}{\mathbf{slope_{std}}} \right)$$

Where the subscripts x and std represents the test compound and standard, respectively and Φ is the fluorescence quantum yield.

A home-made, time-correlated, single-photon counting (TCSPC) instrument with a SPC-630 TCSPC module (Becker & Hickl GmbH) was used to collect the fluorescence time-resolved data (*22*). Scattered light at the center excitation wavelength of 400 nm was collected (without the 450-nm long-pass emission filter used to collect the fluorescence lifetimes) to measure the instrument response function (IRF). Generally, the full-width at half-maximum of the IRF was approximately 50 ps. The TCSPC data were collected in 1024 channels (bins), with a time resolution of 98 ps/channel, and a full-scale time window of 100 ns. The peak-channel counts were set to 65,535. Data were fit with both a single and double exponential curve, and the fit with the lowest chi-square value was considered to be the best fit.

Cell culture: HeLa (Human cervix epithelial cell line) and GM07373 (Bovine endothelial cell line) cell lines were cultured in Dulbecco's Modified Eagle's Medium (DMEM) supplemented with 10% fetal bovine serum, 12.5 mM streptomycin, and 36.5 mM penicillin (Fisher Scientific, Pittsburgh, PA) and incubated in a humidified incubator with 5% CO_2 at 37 ^{o}C (Thermo Scientific, Waltham, MA). These cell cultures were sub-cultured every two days using a 0.25% (w/v) trypsin-EDTA (Life Technology, Carlsbad, CA) solution.

Cell viability assay: The viability of cells treated with Compound **1a** or **1b** was determined using the MTT (3-(4,5-dimethylthiazol-2-yl)-2,5-diphenyltetrazolium bromide) assay. HeLa cells (4×10^4 cells /mL) or GM07373 cells (7×10^4 cells /mL) were treated with concentrations of Compound **1a** or **1b** from 3-1600 μM in complete DMEM medium in a 96 well plate and incubated for 24 h at 37°C. After a 24 h incubation period, MTT in a PBS (5 mg/mL) solution was added to the wells and incubated at 37°C for 3 h. Then the medium was removed from the wells and the formazan crystals were solubilized using a solubilization solution (16% (w/v) sodium dodecyl sulfate (SDS) in 40% (v/v) dimethylformamide (DMF) and 2% (v/v) glacial acetic acid, pH = 4.7). Absorbance was measured at 570 nm to determine the amount of produced formazan in each well. The percent viability was calculated based on the following equation.

$$\textbf{Percent viability} = \frac{\textbf{absorbance of compound 4a or 4b treated well}}{\textbf{absorbance of untreated control well}} \times \textbf{100}$$

The IC50 value (i.e., the concentration of a drug that is required for 50% inhibition of cell viability) was calculated by fitting the dose response curve with the Hill equation (*23*).

Preparation of cells for microscopy studies: HeLa and GM07373 cells were plated on custom-made glass-bottom culture dishes and incubated overnight before performing microscopy experiments. On the day of the microscopy experiment, the growth medium was replaced with 2-5 μM Compound **1a** or **1b** in Hank's Balanced Salt Solution (HBSS) and incubated for 1 h at 37 °C. Cells were rinsed with HBSS medium and microscopy experiments were performed in HBSS medium. GM07373 cells were incubated with Compound **1a** or **1b** in HBSS medium for 1 h at 37 °C then fixed with 4% paraformaldehyde for 10 min. After fixation, they were rinsed and imaged in PBS medium.

Microscopy experiments: Wide-field imaging experiments were performed on a Nikon Eclipse TE2000U microscope (Melville, NY) operating in wide-field epi-fluorescence mode and equipped with a 100× Apo 1.49-numerical-aperture oil-immersion objective. Cell samples were illuminated with a mercury lamp (X-Cite 120 PC, EXFO Photonic Solutions Inc., Mississauga, Ontario, Canada). Compound **1a** and **1b** were excited using a 365 ± 35 nm filter and the signal was collected with a 470 ± 50 nm filter from Omega Optical (Brattleboro, VT). Fluorescence images were collected using a PhotonMAX 512 EMCCD camera (Princeton Instruments, Trenton, NJ) with acquisition times that ranged from 0.4 s to 2 s. Images were further analyzed with ImageJ software (National Institute of Health).

A Leica SP5 X MP inverted confocal microscope was used to collect confocal images. A 405 nm laser was used to excite Compounds **1a** and **1b**. ER-Tracker^{TM} Red was excited with a white light laser passing 580 nm. Emission of Compounds **1a** and **1b** was collected in the range from 460 to 480 nm and that of ER-Tracker^{TM} Red was collected from 610 to 630 nm.

Co-localization experiment for organelle-specific fluorophores: GM07373 cells were simultaneously incubated with Compound **1a** (1 μM) and the organelle-specific fluorophore in HBSS medium for 30 min at 37 ^{o}C. The organelle-specific fluorophores were: 1 μM ER-Tracker^{TM} Red (Invitrogen, Carlsbad, CA), 0.5 μM MitoTracker^{TM} Green FM (Invitrogen, Carlsbad, CA), and 50 nM LysoTracker^{TM} Red DND-99 (Invitrogen, Carlsbad, CA). Then the cells were rinsed and imaged in HBSS medium. Excitation/emission filters passed 365 ± 45 nm/470 ± 20 nm (Compound **1a**), 562 ± 40 nm /629 ± 56 nm (ER-Tracker^{TM} Red), 500 ± 20 nm/535 ± 35 nm (MitoTracker^{TM} Green FM), and 562 ± 40 nm/629 ± 56 nm (LysoTracker^{TM} Red DND-99).

RESULTS AND DISCUSSION

Synthesis and characterization

Compounds **1a** and **1b** were synthesized using a simple, two step reaction (Scheme **1**) and the chemical yields were 47% and 53%, respectively. These compounds were characterized using 1H NMR (Figure **S2**), 13C NMR (Figure **S3**), and high-resolution mass spectrometry (Figure S4). The high-resolution mass spectra of positive ions of Compound 1a and 1b confirmed the molecular masses of the structures (Figure **S4**). The observed mass for Compound 1a was 501.2060 and the calculated mass was 501.2054. The observed and calculated masses for Compound 1b were 517.2002 and 517.2003, respectively.

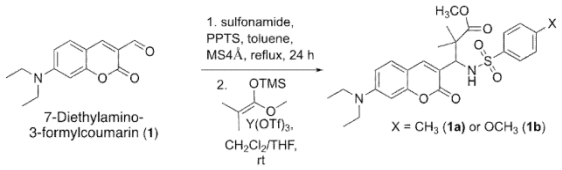

Scheme **1**: Synthetic procedure for Compound 1a and 1b.

The excitation spectra of Compound **1a** and **1b** had a λ_{max} of 410 nm, and the emission spectra had a λ_{max} of 486 ± 1 nm in water (Figure **1**). For both compounds, the full-width at half-maximum was 62 ± 1 nm for the fluorescence spectrum, and fluorescence quantum yields were measured as 0.60 using coumarin 153 as a standard. Compounds **1a** and **1b** had extinction coefficients of 29,530 $M^{-1}cm^{-1}$ and 25,100 $M^{-1}cm^{-1}$, respectively.

Cell viability assay

The cytotoxicity of Compounds **1a** and **1b** in GM 07373 and HeLa cells was evaluated using an MTT assay (Figure **S5**). The half maximal inhibitory concentrations (IC_{50}) were detected as 215 ± 2 μM (Compound **1a**) and 252 ± 2 μM (Compound **1b**) for GM 07373 cells. The IC_{50} of

Compound **1a** and **1b** for the HeLa cell line were 205 ± 2 μM and 239 ± 1 μM, respectively. These IC_{50} values were significantly higher than the concentrations of the probes used for imaging studies (0.5-5 μM), indicating the compounds exhibit negligible toxicity at concentrations relevant for imaging experiments within these tested cell lines. Trypan Blue exclusion assays were used to check the cell viability in HBSS medium over the timescales relevant for the imaging experiment (Supplementary page 3). The results (Table **S1**) show there is no significant difference between the cell viability of **1a** or **1b** treated cells and the control cells. The low cytotoxicity under imaging conditions means these probes are applicable for live cell studies.

Microscopy experiments showing localization to the ER

Based on the presence of the sulfonamide group and the coumarin structure, Compounds **1a** and **1b** were hypothesized to be ER-targeting fluorescent probes. In order to test this, HeLa and GM07373 cells were incubated with 2 μM Compounds **1a** or **1b**, and live cells were imaged using a wide-field microscope. Both compounds penetrated the cell membrane and produced a fluorescence signal that was mainly observed in the perinuclear region of the cells, targeted to a tubular structure (Figure **2**). As a control experiment, HeLa and GM07373 cells were incubated with 2 μM 7-diethylamino-3-formylcoumarin and live cells were imaged. As shown in figure **S6**, the fluorescent signal was observed inside the cell but did not localized into any specific intracellular structure. This observation supports the hypothesis that the sulfonamide side group in Compound **1a** and **1b** is essential for targeting the probe into the ER.

<Figure 2>

Co-localization experiments were performed using commercially available organelle trackers to identify the intracellular location of Compound **1a** (Figure **3**). The GM07373 cell images corresponding to the emission signal of ER-Tracker™ Red and that of the Compound **1a** were well overlapped and the Pearson's correlation coefficient was 0.94. Images of cells labeled with MitoTracker™ Green FM and LysoTracker™ Red DND-99 fluorophores were not well overlapped with the images corresponding to Compound **1a** and the Pearson's correlation coefficients were 0.37 and 0.29, respectively.

<Figure 3>

The results for Compound **1b** were consistent with Compound **1a** (Figure **S7)**. Confocal microscopy images, which have improved axial spatial resolution compared to wide-field microscopy, also indicate that Compound **1a** and **1b** colocalize with known ER probes within the cells (Figure **S8** and **S9**). A movie of a live GM07373 cell treated with Compound **1a** is provided in the supplementary information, and highlights the ability to visualize the dynamics of the ER structure with this probe.

We further examined the compatibility of these compounds with fixation protocols. The fluorescence signal corresponding to Compound **1a** and **1b** were detected in the ER region even after fixation with 4% formaldehyde (Figure **4**).

<Figure 4>

Effects of solvent polarity on optical properties

The absorption and emission spectra of the Compound **1a** and **1b** were measured in solvents with various polarities (Figure **S10**). In water, both probes showed the maximum absorption at 410 nm and maximum fluorescence at 486 ± 1 nm, as discussed above. When the polarity of

the solvent decreased, the absorption and fluorescence emission curves were blue shifted. The λ_{max} of fluorescence was: 467 nm in methanol, 457 nm in DMSO, 444 nm in methylene chloride and 432 nm in toluene. The bathochromic shift of the absorption and fluorescence spectra with increased solvent polarity is consistent with reports in literature for 7-alkylamino coumarins (*24, 25*). For the higher polarity solvents, the lower energy of the excited state fluorophore is due to the relaxation or reorientation of the excited state by the solvent dipoles (*26*). The fluorescence spectra measured for Compound **1a** and **1b** inside the cells were compatible with the fluorescence spectra collected in methanol or DMSO (Figure **5**).

<Figure 5>

This observation is consistent with Compound **1a** and **1b** being targeted to the ER membrane, which is less polar than the cytoplasm but not as nonpolar as the cell membrane due to its lower cholesterol concentration (*14*). In addition, the cLogD values reporting the partitioning between n-octanol and water were 4.2 and 3.8 for Compounds **1a** and **1b,** respectively. These values are consistent with other ER labeling probes (e.g., the cLogD of ER-Tracker™ Blue-White DPX is 4.0), and indicate the hydrophobic nature of these compounds make them compatible for partitioning into the ER membrane environment.

In order to show the utility of Compounds **1a** and **1b** for fluorescence lifetime imaging (FLIM), their lifetimes were also measured using the time-correlated single-photon counting (TCSPC) method (Figure **S11**). In an aqueous medium, data collected for both probes were well fit to a double exponential decay with average lifetimes of 1.55 and 1.56 ns for Compound **1a** and **1b,** respectively. Approximately 90% of the population had a shorter lifetime (about 1.46 ns). About 10% of the population had lifetimes of 2.56 ns for Compound **1a** and 2.31 ns for Compound **1b**. The observation of two decay components in water is

comparable to the results observed for 7-(diethylamino)coumarin-3-carboxylic acid molecule (*27*). In a high-polar protic medium, a planer intramolecular charge-transfer (ICT) excited state can be changed to a twisted charge transfer (TICT) excited state by rotating the bond orientation at the 7-diethylamino group of the probe. The ICT excited state is highly emissive but the TICT excited state undergoes nonradiative decay and is nonfluorescent (*24*). These two excited state populations likely explain the two populations measured in water. The lifetime data collected for Compound **1a** and **1b** in less polar aprotic and nonpolar solvents were well fit to a single exponential decay curve. In less polar aprotic solvents both the ground and excited states are likely in planer ICT structures (*28*) and the resulting lifetimes were 3.66 to 3.41 nm for Compound **1a** and 3.68 to 3.44 ns for Compound **1b**. In nonpolar solvents like toluene, 7-diethylamino group adopts a pyramidal configuration and forms a nonplanar structure in the ground and excited states (*28*). Therefore the observed lifetimes in toluene (2.94 nm for Compound **1a** and 2.99 ns for Compound **1b)** were lower than that of less polar aprotic solvents ((Figure **S11**). The lifetime of Compound **1a** and **1b** could not be measured in the cellular environment with the available instrument, however, the results discussed above suggest that the probes are suitable for FLIM and may report on the environment of the probe.

CONCLUSION

Two coumarin derivatives were synthesized, characterized and their optical properties were evaluated as ER targeting probes in live and fixed mammalian cells. The synthetic procedure is not complex with only two involved steps. These compounds have comparable hydrophobicities as commercially available ER probes. A bright and narrow emission profile in the blue region (from 435-525 nm in methanol) was detected with excitation around 400

nm, indicating that these probes will be suitable for multi-color imaging with other probes. In these studies, there was no measureable difference in the membrane permeability of 1a and 1b in the tested cell lines. The quantum yields were also the same for both compounds, but 1a has a slightly higher extinction coefficient than that of 1b. Therefore, compound 1a has a slightly higher quantum efficiency (i.e., quantum yield times extinction coefficient). To further enhance the applicability of these probes in multi-color imaging, a series of ER probes with varying absorption/emission profiles could be developed by extending the conjugation in the coumarin core.

ACKNOWLEDGMENTS*:* This work was initiated with funding from NSF grant CHE-1412084 and continued with funding from NSF grant CHE-1709099. We acknowledge the technical assistance from ISU Chemical Instrumentation Facility staff member Dr. K. Harrata for the mass spectroscopy measurements, the W. M. Keck Metabolomics Research Laboratory at Iowa State University for the use of their micro-plate reader, and Dr. J. Petrich and Dr. K. Santra for their assistance with the time-correlated, single-photon counting measurements.

SUPPLEMENTARY MATERIALS

Figures S1 to S11, ^{1}H & ^{13}C NMR characterization of **1a** and **1b**, and supplementary movie can be found at DOI: 10.1562/2006-xxxxxx.s1.

REFERENCES

1. Cooper, G. M. (2000) Endoplasmic Reticulum, in *The Cell: A Molecular Approach.* Second ed., Sinauer Associates, Sunderland (MA).
2. Schwarz, D. S., and Blower, M. D. (2016) The endoplasmic reticulum: structure, function and response to cellular signaling, *Cell Mol Life Sci 73*, 79-94.
3. Voeltz, G. K., Rolls, M. M., and Rapoport, T. A. (2002) Structural organization of the endoplasmic reticulum, *EMBO Rep 3*, 944-950.
4. Braakman, I., and Bulleid, N. J. (2011) Protein folding and modification in the mammalian endoplasmic reticulum, *Annu Rev Biochem 80*, 71-99.
5. Vance, J. E. (2015) Phospholipid synthesis and transport in mammalian cells, *Traffic 16*, 1-18.
6. He, H., Lam, M., McCormick, T. S., and Distelhorst, C. W. (1997) Maintenance of calcium homeostasis in the endoplasmic reticulum by Bcl-2, *J Cell Biol 138*, 1219-1228.
7. Sovolyova, N., Healy, S., Samali, A., and Logue, S. E. (2014) Stressed to death - mechanisms of ER stress-induced cell death, *Biol Chem 395*, 1-13.
8. Schuck, S., Prinz, W. A., Thorn, K. S., Voss, C., and Walter, P. (2009) Membrane expansion alleviates endoplasmic reticulum stress independently of the unfolded protein response, *J Cell Biol 187*, 525-536.
9. van Bergeijk, P., Hoogenraad, C. C., and Kapitein, L. C. (2016) Right Time, Right Place: Probing the Functions of Organelle Positioning, *Trends Cell Biol 26*, 121-134.
10. Guiot, Y., Stevens, M., Marhfour, I., Stiernet, P., Mikhailov, M., Ashcroft, S. J. H., Rahier, J., Henquin, J. C., and Sempoux, C. (2007) Morphological localisation of sulfonylurea receptor 1 in endocrine cells of human, mouse and rat pancreas, *Diabetologia 50*, 1889-1899.
11. Tang, Y., Xu, A., Ma, Y., Xu, G., Gao, S., and Lin, W. (2017) A turn-on endoplasmic reticulum-targeted two-photon fluorescent probe for hydrogen sulfide and bio-imaging applications in living cells, tissues, and zebrafish, *Sci Rep 7*, 12944.

12. Xiao, H. B., Li, P., Hu, X. F., Shi, X. H., Zhang, W., and Tang, B. (2016) Simultaneous fluorescence imaging of hydrogen peroxide in mitochondria and endoplasmic reticulum during apoptosis, *Chem Sci 7*, 6153-6159.
13. Xu, S., Liu, H. W., Hu, X. X., Huan, S. Y., Zhang, J., Liu, Y. C., Yuan, L., Qu, F. L., Zhang, X. B., and Tan, W. (2017) Visualization of Endoplasmic Reticulum Aminopeptidase 1 under Different Redox Conditions with a Two-Photon Fluorescent Probe, *Anal Chem 89*, 7641-7648.
14. van Meer, G., and de Kroon, A. I. (2011) Lipid map of the mammalian cell, *J Cell Sci 124*, 5-8.
15. Arai, S., Lee, S. C., Zhai, D., Suzuki, M., and Chang, Y. T. (2014) A molecular fluorescent probe for targeted visualization of temperature at the endoplasmic reticulum, *Sci Rep 4*, 6701.
16. Yang, Z., He, Y., Lee, J. H., Chae, W. S., Ren, W. X., Lee, J. H., Kang, C., and Kim, J. S. (2014) A Nile Red/BODIPY-based bimodal probe sensitive to changes in the micropolarity and microviscosity of the endoplasmic reticulum, *Chem Commun (Camb) 50*, 11672-11675.
17. Terasaki, M., Song, J., Wong, J. R., Weiss, M. J., and Chen, L. B. (1984) Localization of endoplasmic reticulum in living and glutaraldehyde-fixed cells with fluorescent dyes, *Cell 38*, 101-108.
18. Soltys, B. J., and Gupta, R. S. (1992) Interrelationships of endoplasmic reticulum, mitochondria, intermediate filaments, and microtubules--a quadruple fluorescence labeling study, *Biochem Cell Biol 70*, 1174-1186.
19. Cole, L., Davies, D., Hyde, G. J., and Ashford, A. E. (2000) Brefeldin A affects growth, endoplasmic reticulum, Golgi bodies, tubular vacuole system, and secretory pathway in Pisolithus tinctorius, *Fungal Genet Biol 29*, 95-106.
20. Cole, L., Davies, D., Hyde, G. J., and Ashford, A. E. (2000) ER-Tracker dye and BODIPY-brefeldin A differentiate the endoplasmic reticulum and golgi bodies from the tubular-vacuole system in living hyphae of Pisolithus tinctorius, *J Microsc 197*, 239-249.

21. Zimmerman, J. R., Johntony, O., Steigerwald, D., Criss, C., Myers, B. J., and Kinder, D. H. (2015) The Synthesis of a New Class of Highly Fluorescent Chromones via an Inverse-Demand Hetero-Diels-Alder Reaction, *Org Lett 17*, 3256-3259.
22. Santra, K., Smith, E. A., Petrich, J. W., and Song, X. (2017) Photon Counting Data Analysis: Application of the Maximum Likelihood and Related Methods for the Determination of Lifetimes in Mixtures of Rose Bengal and Rhodamine B, *J Phys Chem A 121*, 122-132.
23. Motulsky, H., Christopoulos, A. (2004) Fitting Dose Response Curves, in *Fitting Models to Biological Data Using Linear and Nonlinear Regression, A practical guide to curve fitting*, pp 256-265, Oxford University Press, New York.
24. Jones, G., Jackson, W. R., Choi, C., and Bergmark, W. R. (1985) Solvent Effects on Emission Yield and Lifetime for Coumarin Laser-Dyes - Requirements for a Rotatory Decay Mechanism, *J Phys Chem-Us 89*, 294-300.
25. Reichardt, C. (1994) Solvatochromic Dyes as Solvent Polarity Indicators, *Chem Rev 94*, 2319-2358.
26. Lakowicz, J. R. (2006) Solvents and Environmental Effects, in *Principles of Fluorescence Spectroscopy* Third ed., pp 205-231, Springer Science+Business Media, New York.
27. Chatterjee, A., and Seth, D. (2013) Photophysical properties of 7-(diethylamino)coumarin-3-carboxylic acid in the nanocage of cyclodextrins and in different solvents and solvent mixtures, *Photochem Photobiol 89*, 280-293.
28. Senthilkumar, S., Nath, S., and Pal, H. (2004) Photophysical properties of coumarin-30 dye in aprotic and protic solvents of varying polarities, *Photochem Photobiol 80*, 104-111.

FIGURE CAPTIONS

Figure 1: (A) Structures of coumarin-based Compounds **1a** and **1b**. The normalized excitation and fluorescence spectra of (B) Compound **1a** and (C) Compound **1b**.

Figure 2: Images of (A, B, C) live HeLa cells and (D, E, F) live GM07373 cells treated with (A & D) 2 μM Compound 1a, (B & E) 2 μM Compound 1b and (C & F) control showing cellular autofluorescence. All images are shown in the same intensity scale. Scale bar is 20 μm in all the images.

Figure 3: Images of live GM07373 cells co-labeled with Compound **1a** and commercially available organelle-specific fluorophores. The images A, C and E show the fluorescence signal corresponding to Compound **1a**. The images B, D and F show the fluorescence signal from ER-Tracker™ (endoplasmic reticulum), MitoTracker™ (mitochondria) and LysoTracker™ (lysosomes), respectively. The yellow color in the images in the right column shows where there is overlap in the signal for Compound **1a** and the organelle specific fluorophore. Scale bar is 20 μm in all the images.

Figure 4: Images of GM07373 cells incubated with (A) Compound **1a** and (B) Compound **1b** for 1 h and then fixed with 4% paraformaldehyde. Scale bar is 20 μm in both images.

Figure 5: Normalized fluorescence spectra of (A) Compound **1a** and (B) Compound **1b** dissolved in solvents with different polarities (solid lines) and inside the HeLa cells as measured by microspectroscopy (dotted lines).

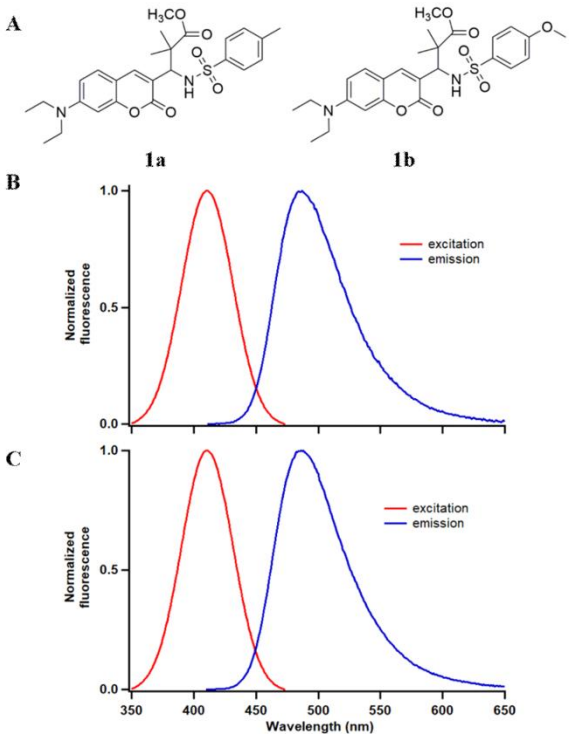

Figure 1: (A) Structures of coumarin-based Compounds **1a** and **1b**. The normalized excitation and fluorescence spectra of (B) Compound **1a** and (C) Compound **1b**.

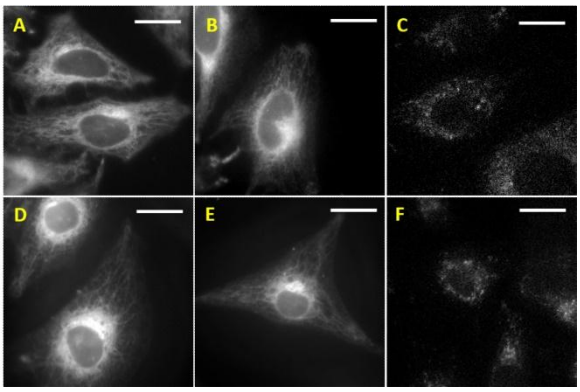

Figure 2: Images of (A, B, C) live HeLa cells and (D, E, F) live GM07373 cells treated with (A & D) 2 μM Compound 1a, (B & E) 2 μM Compound 1b and (C & F) control showing cellular autofluorescence. All images are shown in the same intensity scale. Scale bar is 20 μm in all the images.

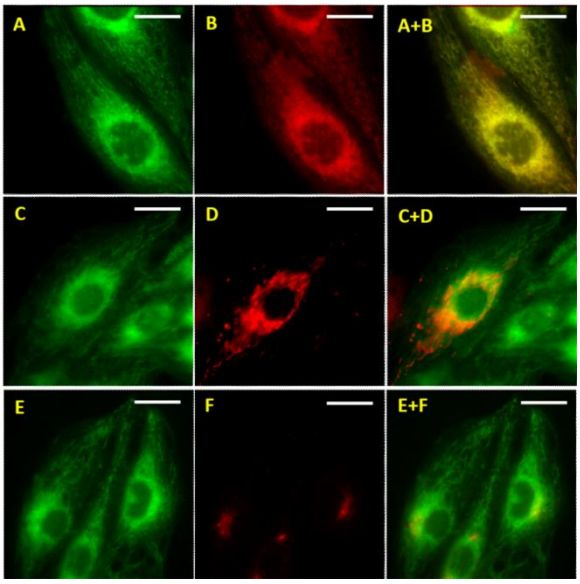

Figure 3: Images of live GM07373 cells co-labeled with Compound **1a** and commercially available organelle-specific fluorophores. The images A, C and E show the fluorescence signal corresponding to Compound **1a**. The images B, D and F show the fluorescence signal from ER-Tracker™ (endoplasmic reticulum), MitoTracker™ (mitochondria) and LysoTracker™ (lysosomes), respectively. The yellow color in the images in the right column shows where there is overlap in the signal for Compound **1a** and the organelle specific fluorophore. Scale bar is 20 μm in all the images.

1 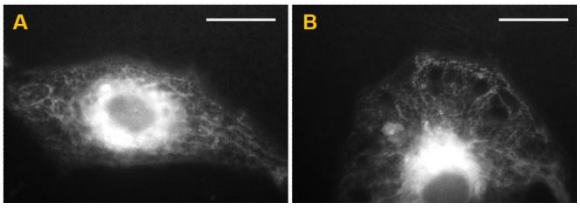

2 **Figure 4**: Images of GM07373 cells incubated with (A) Compound **1a** and (B) Compound **1b**

3 for 1 h and then fixed with 4% paraformaldehyde. Scale bar is 20 μm in both images.

4

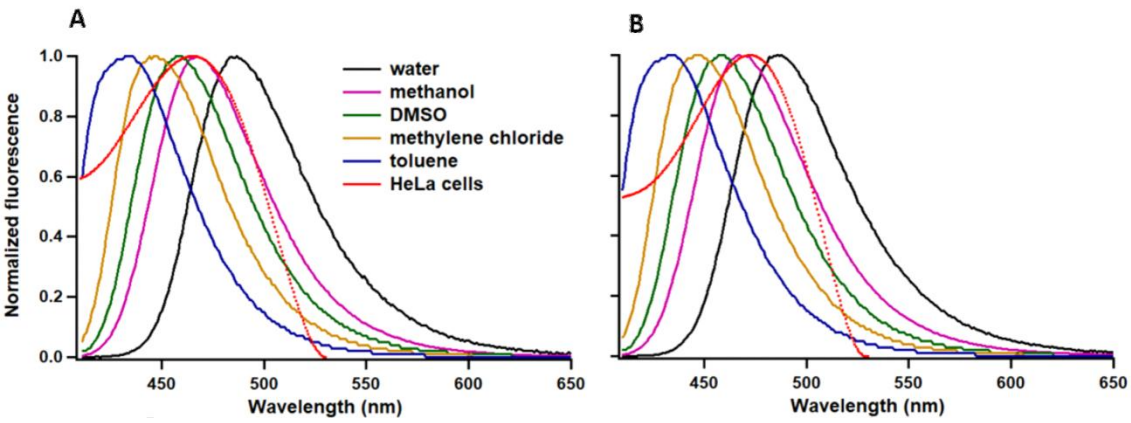

Figure 5: Normalized fluorescence spectra of (A) Compound **1a** and (B) Compound **1b** dissolved in solvents with different polarities (solid lines) and inside the HeLa cells as measured by microspectroscopy (dotted lines).